

# As-grown bulk lifetime: Increasingly relevant for silicon solar cell performance

Bernhard Mitchell<sup>1</sup>, Daniel Chung<sup>1</sup>, Zhen Xiong<sup>2</sup>, Pietro P. Altermatt<sup>2</sup>, Peter Geelan-Small<sup>1</sup> & Thorsten Trupke<sup>1,3</sup>

<sup>1</sup>University of New South Wales, Sydney, Australia; <sup>2</sup>State Key Laboratory of PV Science and Technology, Trina Solar, Changzhou, Jiangsu, PR China; <sup>3</sup>BT Imaging Pty Ltd, Sydney, Australia

## Abstract

This paper investigates the influence of the as-grown silicon material quality on the performance of multicrystalline silicon passivated emitter and rear solar cells (PERCs), using recently developed spectral photoluminescence (PL) imaging techniques at the ingot level (i.e. on silicon bricks), and testing these cells in conjunction with PL measurements on as-cut wafers. The effects of material properties – including bulk lifetime, dislocation density and resistivity – are studied with regard to their correlation to cell output over the whole sample set of three directionally solidified production bricks of widely varying bulk lifetimes and dislocation densities. The data are analysed statistically using a linear mixed model. Bulk lifetime is observed to be correlated to cell performance throughout the studied sample set. The strength of the correlation is determined to be greatest for the material with low dislocation density, where a linear correlation between cell performance and as-grown bulk lifetime is found. There is a clear ongoing trend for increases in cell efficiency and for decreases in the area of dislocations in multicrystalline wafers. Because of this progression, bulk lifetime measured only on the bricks is well suited to predicting the often-dominant material-related variations in cell performance before cell fabrication.

### Silicon material quality parameters: bulk lifetime, dislocation density, resistivity

By the end of 2017 it is expected that boron-doped multicrystalline silicon (p-type mc-Si) wafers will have been used in more than 60% of the world's manufactured solar cells [1]. Low-cost mc-Si can be crystallized in large ingots with high throughputs and with less oxygen built into the crystal than in the case of Czochralski-grown monocrystalline silicon (Cz-Si). However, mc-Si contains extended defects (mainly grain boundaries and dislocations) and a higher concentration of metal contaminants. These types of defect usually cause lower as-grown excess carrier lifetimes in mc-Si than in Cz-Si. Both Cz-Si and mc-Si can be affected by degradations of the excess carrier lifetime during module operation in the field [2,3], if defect formation processes are not regenerated or passivated [4,5].

“A prediction of efficiency from the as-grown silicon material would be extremely valuable in terms of enabling further optimization of production and the identification of R&D priorities.”

With improvements in the emitter in standard cells, and with the passivated emitter and rear cell (PERC) being introduced into mass production, bulk recombination is becoming increasingly limiting to achievable cell efficiency [6,7], particularly when using p-type mc-Si wafers [8]. In much of today's mc-Si material, the excess carrier lifetime is limited by dislocations that remain active in the final device, even after gettering and hydrogenation steps [9,10]. However, in recent years the dislocation density of mc-Si has been reduced through advanced engineering of the growth process and the control of the grain size, which (along with improved quartz crucible technology) have also improved bulk lifetimes. As an example, effective lifetimes exceeding 500 $\mu$ s at an injection level of  $10^{15}$ cm<sup>-3</sup> have been measured on p-type mc-Si with surface passivation, after removal of the phosphorus-diffused layers on both sides [11].

A recent study confirmed that a significant proportion of the total variance in mc-Si PERC cell efficiency is due to bulk lifetime [12]. The question arises as to whether much of this variance can be predicted from the as-grown silicon material, noting that the Si material is altered during cell processing, for example by gettering and annealing during phosphorus diffusion and through hydrogen bulk passivation. A prediction of efficiency from the as-grown silicon material would be extremely valuable in terms of enabling further optimization of production (selective processing, sorting, optimization of the crystallization processes, etc.) and the identification of R&D priorities.

The three most important material quality metrics in mc-Si are:

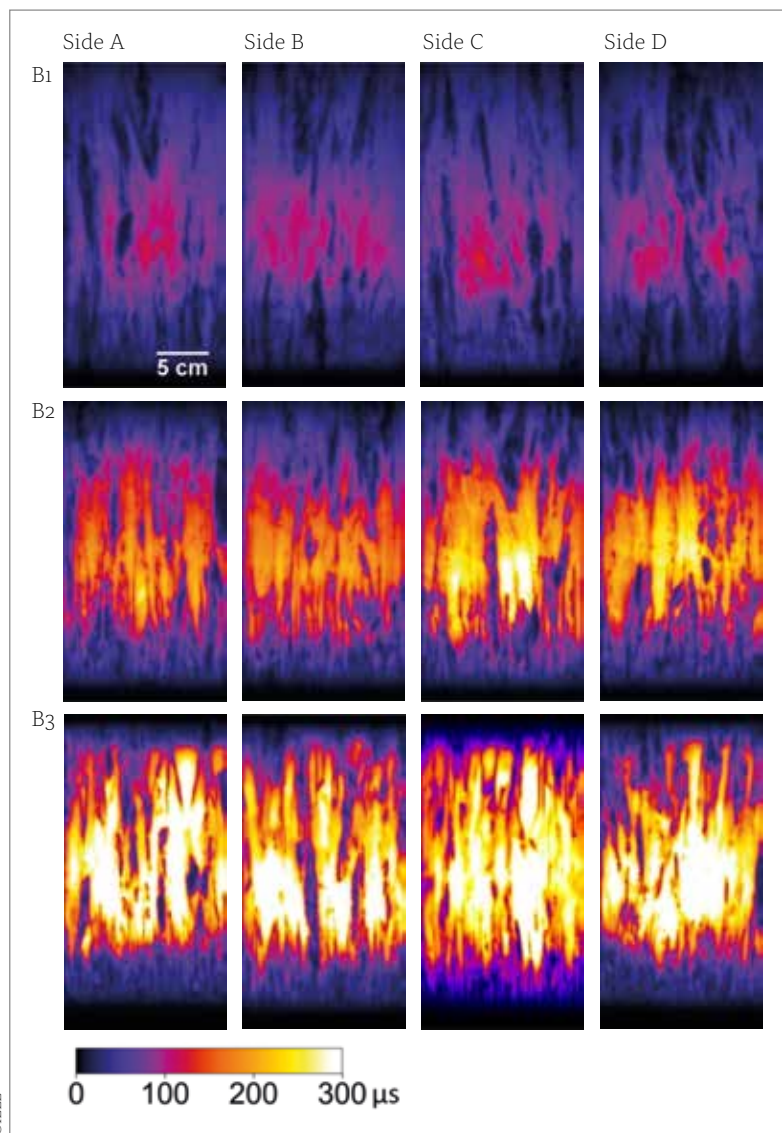
1. Excess carrier bulk lifetime (for simplicity denoted 'lifetime' hereafter)
2. Dislocation area fraction
3. Resistivity

It should be stressed that all measurements of lifetime in this study relate to as-grown material and not to the effective or bulk lifetime of silicon

## “The sPLIR technique defines a new standard for industrial metrology at the ingot level.”

after solar cell processing. The dislocation area fraction can be measured accurately on as-cut wafers using PL imaging, while the resistivity can be measured with an eddy-current sensor. However, the bulk lifetime of as-cut wafers cannot be accurately determined from effective lifetime measurements, since the strong surface recombination causes an asymptotic relationship between the bulk and the effective lifetime for values above  $\sim 10\mu\text{s}$  [13]. However, bulk lifetime can be measured on bricks, since this material property is associated with a spectral shift in the PL emission spectrum [14]. Additionally, the resistivity can be readily measured on bricks. It should be noted that the dislocation area fraction across the surface of wafers is not very representative of dislocation area fractions on the side facets of bricks.

**Figure 1. Bulk lifetime images of each of the four sides of three bricks, using the spectral PL intensity ratio analysis (sPLIR) [16]. The colour scale ranges from 0 to  $300\mu\text{s}$  and is identical for all images. The weighted average injection level is in the range  $1\text{--}8 \times 10^{13}\text{cm}^{-3}$ , depending on the local lifetime. Each brick facet is approximately  $156\text{mm} \times 315\text{mm}$  in size.**



Measurements of dislocation area fractions on as-cut wafer have previously been used to fairly accurately predict cell performance [9]. This approach has worked particularly well for Al-BSF cells, as the performance of these cells is commonly not limited by the bulk lifetime or the respective diffusion length within the larger grains [8,15]. Thus, any variances in cell performance are primarily caused by extended defects, i.e. dislocations and grain boundaries, which act to significantly reduce the lifetime, carrier collection and implied voltage locally. The performance of mc-Si PERC solar cells has been predicted using this approach, but with larger absolute errors, however, because of the stronger influence of bulk lifetime [9]. To the authors' knowledge, predictions of cell efficiencies based on lifetime measurements from PL imaging on bricks have not been published prior to this work. However, Gibaja et al. [16] studied quality metrics based on quasi-steady state photoconductance (QSSPC) measurements on ingots.

The study reported in this paper combines recent advances in ingot PL imaging achieved at UNSW and BT Imaging [17,18], with state-of-the-art high-performance multi material and cell production at Trina Solar [11]. It is shown to what certainty variances in material properties, as measured in silicon bricks, can be used to predict cell performance. In particular, the specific material properties (lifetime, dislocation and resistivity) that have the strongest correlation to cell efficiencies in industrial production are investigated. This paper is an extract of the full paper published by Mitchell et al. [19].

### Combining brick, wafer and cell metrology data

Three bricks with a large spread of values in bulk lifetime and dislocation area fractions were selected from the production line at Trina Solar. The bricks originated from different silicon ingots, giving three completely independent samples. Each brick was measured on all four side facets using BT Imaging's LIS-B3 brick inspection tool [20], which utilizes the patented quantitative spectral photoluminescence intensity ratio analysis technique (sPLIR) [14]. In this method, steady-state bulk lifetime images are acquired using a line-scanning photoluminescence (PL) imaging system at an injection level that depends on the bulk lifetime, for example  $3 \times 10^{13}\text{cm}^{-3}$  at  $1\mu\text{s}$  and  $8 \times 10^{13}\text{cm}^{-3}$  at  $500\mu\text{s}$ , which reflects the depth-weighted average bulk lifetime across the outer 1–3mm of the brick [14]. The sPLIR technique has been developed and refined over the last seven years by UNSW and BT Imaging, and defines a new standard for industrial metrology at the ingot level.

Height-dependent bulk lifetime measurements were made on all four facets of each of the bricks. These bulk lifetime profiles provide a single lifetime value for each wafer position (given as the distance from the bottom of the ingot) by appropriately

averaging the bulk lifetime data over the four sides of the brick. In this study, an image resolution of 320µm per pixel was used to assess the spatially resolved bulk lifetime, resulting in about 1000 data points along the height of the brick. In addition, resistivity measurements along the height profile were taken on all four sides of the bricks.

Fig. 1 outlines the significant spread in material quality that is present across the sampled bricks, with maximum intra-grain bulk lifetimes of up to 120µs in B1, 250µs in B2 and almost 450µs in B3. The appearance of dark features in the bulk lifetime images also indicates that B1 has more dislocations than B2 and B3.

The three bricks were subsequently cropped, polished and sliced into wafers. The wafers were fully tracked, and every fifth wafer was processed into PERC solar cells at Trina Solar. The  $I-V$  parameters ( $I_{sc}$ ,  $V_{oc}$ ,  $FF$ , etc.) of the cells were measured using a production xenon flash lamp  $I-V$  tester. The  $I-V$  data was then matched with the brick and wafer metrology data as a function of brick number and height.

As-cut wafers were characterized using a BT Imaging QS-W3 wafer inspection tool, and a dislocation value was extracted for every wafer using the tool's proprietary image processing algorithms (in a similar fashion to that described by Demant et al. [9]). The dislocation value is proportional to the area fraction of the dislocations in the wafers.

Between the sample sets, a wide spread of dislocation area fractions can be observed (see Fig. 2). Brick B1 is found to have the most dislocations and the lowest lifetimes. This negative correlation between lifetime and dislocation area fraction is also observed in B2 and B3. Remarkably, a negligible dislocation area fraction is found throughout most of brick B3, which shows significant dislocations only in the top 20%.

Fig. 3 shows the height dependence of the profiles for bulk lifetime from PL measurements on bricks, the dislocation area fractions from wafer PL measurements, and the cell efficiencies (normalized to maximum efficiency). Similar trends for bulk lifetime, with a peak near the centre of the brick, are observed for all samples. The shapes of these profiles are a result of the dynamics of segregation and precipitation of transition metals, and the incorporation of light elements (O, C, N) and their silicides into the crystal [25,26] during solidification of the brick.

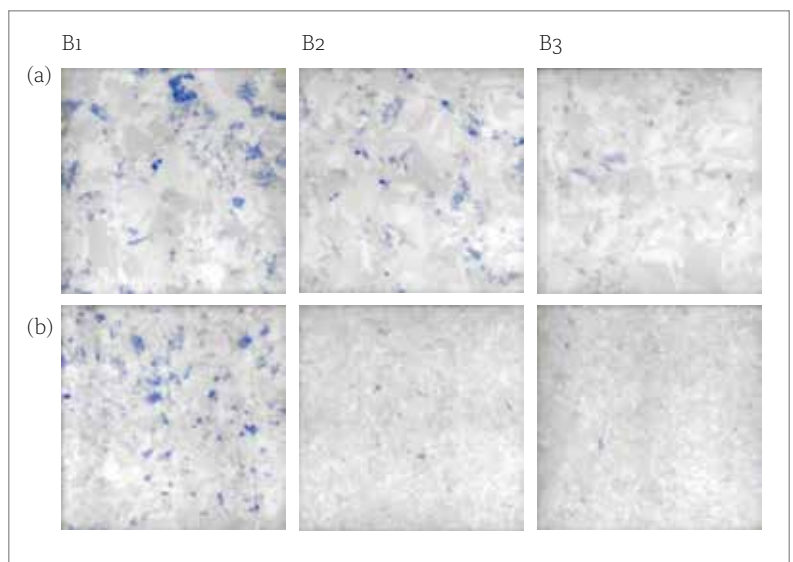
The dislocation profiles for bricks B2 and B3 show the typical trend, with increasing area fractions towards the top of the brick, reflecting the increasing stress release during crystal growth. Brick B1, however, reveals a different dislocation profile, with a minimum at the centre of the brick; the reasons for this unusual observation are unknown to the authors. It is noted that the availability of a large sample set mainly from the

bottom half of brick B3, which is virtually free of dislocations, provides a good set of data for the fitting of the model, with the intention of exploring the correlations between bulk lifetime and cell efficiencies, free of the potentially coupled variable that is represented by dislocations.

Cells produced from this experiment achieved maximum efficiencies well above 19%. The peak cell efficiencies are found in the bottom to middle height position of the bricks for B2 and B3, while B1 exhibits only small changes throughout the height profile, except at the very bottom and top. The efficiencies of B1 are determined to be approximately 3% lower than for both B2 and B3. Mean and peak efficiencies are similar for B2 and B3, despite the differences in as-grown lifetimes and dislocation area fractions.

Since there is a clear qualitative correlation between bulk lifetime and cell efficiency in Fig. 3, the cell efficiencies have been plotted as a function of bulk lifetime and are shown in Fig. 4. A linear fit was applied to the entire dataset (bricks 1–3) and a separate linear fit to only the dislocation-free wafers from brick 3. Both fits have a positive gradient with a similar slope, indicating that areas with increased bulk lifetime in the bricks lead to higher cell efficiencies, as expected. The residuals have a significant spread around the fitted line, which indicates that predictions may not be very accurate at the individual wafer level. The residuals along the fitted line are more evenly spread for the dislocation-free wafers, whereas more significant outliers exist at low lifetimes when fitting to the entire dataset. These outliers are in the heavily dislocated wafers of brick 1. These results suggest that a simple linear correlation between cell efficiency and bulk lifetime from brick measurements is sufficient, although the presence of dislocations may complicate the analysis, since dislocations may impact cell efficiency by a second

**Figure 2. Dislocation structures for bricks 1–3, derived from PL imaging on as-cut wafers: typical raw PL images with defect overlay (blue) for the upper half (a) and the lower half (b) of each brick.**



mechanism that is independent of the impact of dislocations on bulk lifetime.

The linear fit in Fig. 4 is in contrast to the simulated cell performance curves (i.e. cell bulk lifetime as a function of cell efficiency) for typical PERC solar cells, which are non-linear [27]. One important difference between Fig. 4 and typical simulated cell performance curves is the  $x$  axis, which is the as-grown bulk lifetime in Fig. 4, and cell bulk lifetime in the case of typical simulation curves. An improvement in the 'real' bulk lifetime is expected after cell processing because of the gettering effect of the diffusion process and the hydrogenation effect after firing with a silicon nitride layer; therefore, the as-grown bulk lifetime is not expected to follow the same correlation to cell efficiency as that for cell bulk lifetime. Respectable cell efficiencies are achieved even for very low-quality sections of the brick (see Fig. 4), as a result of substantial improvements in bulk lifetime during cell processing.

#### A deeper understanding through statistical modelling

To further investigate the relationship between the measured material-quality variables and the  $I$ - $V$  parameters of the fabricated PERC cells, a model was developed using the statistical analysis

package R [21]. The cell's 1-sun  $I_{sc} \times V_{oc}$  product was selected as the designated *response variable*, since it was desired to focus the analysis on lifetime and dislocation predictors, and to avoid the strong dependence of efficiency on the  $FF$ , which in turn is highly dependent on the base resistivity and the metallization. A similar line of argument can be applied to other  $I$ - $V$  parameters (e.g.  $V_{oc}$ ) [9,12]. Using the  $I_{sc} \times V_{oc}$  product also significantly reduces the impact of processing-related variations, e.g. series resistance and shunt resistance.

A linear mixed model [22,23] is used to fit the relationship between the response variable  $I_{sc} \times V_{oc}$  and the measured metrology data, with a normal distribution assumption, using the package 'nlme' in R [24]. This approach is used instead of an ordinary least-squares multiple linear-regression approach, since the response data, i.e. the solar cell's  $I_{sc} \times V_{oc}$  products, are clustered within bricks, and additionally a non-uniform within-brick correlation structure is expected. Hence these values cannot be regarded as independent of each other, especially if the wafers originate from an approximately similar location within the same brick.

Three models for various types of relationship (lifetime only, dislocation metric from wafer measurements only, and a combination of the two) were used to fit the data. Each model included a

## The LIS-B3: Identify your high efficiency silicon

“ The ideal tool for quality control and process development in silicon brick and ingot manufacturing



[www.btimaging.com](http://www.btimaging.com)

**BT imaging**  
INNOVATE. CONTROL. YIELD.

- > High resolution photoluminescence imaging data with unmatched image quality
- > Incorporating BT Imaging's patented scanning photoluminescence imaging technology
- > Applicable to all types of crystalline silicon ingots and bricks
- > Quantitative high-resolution **bulk** lifetime images from 1  $\mu$ s to 20 ms
- > Cutting guides for multi-crystalline silicon bricks
- > Automatic algorithms report various defect and quality metrics
- > Configurable for manual or automatic loading



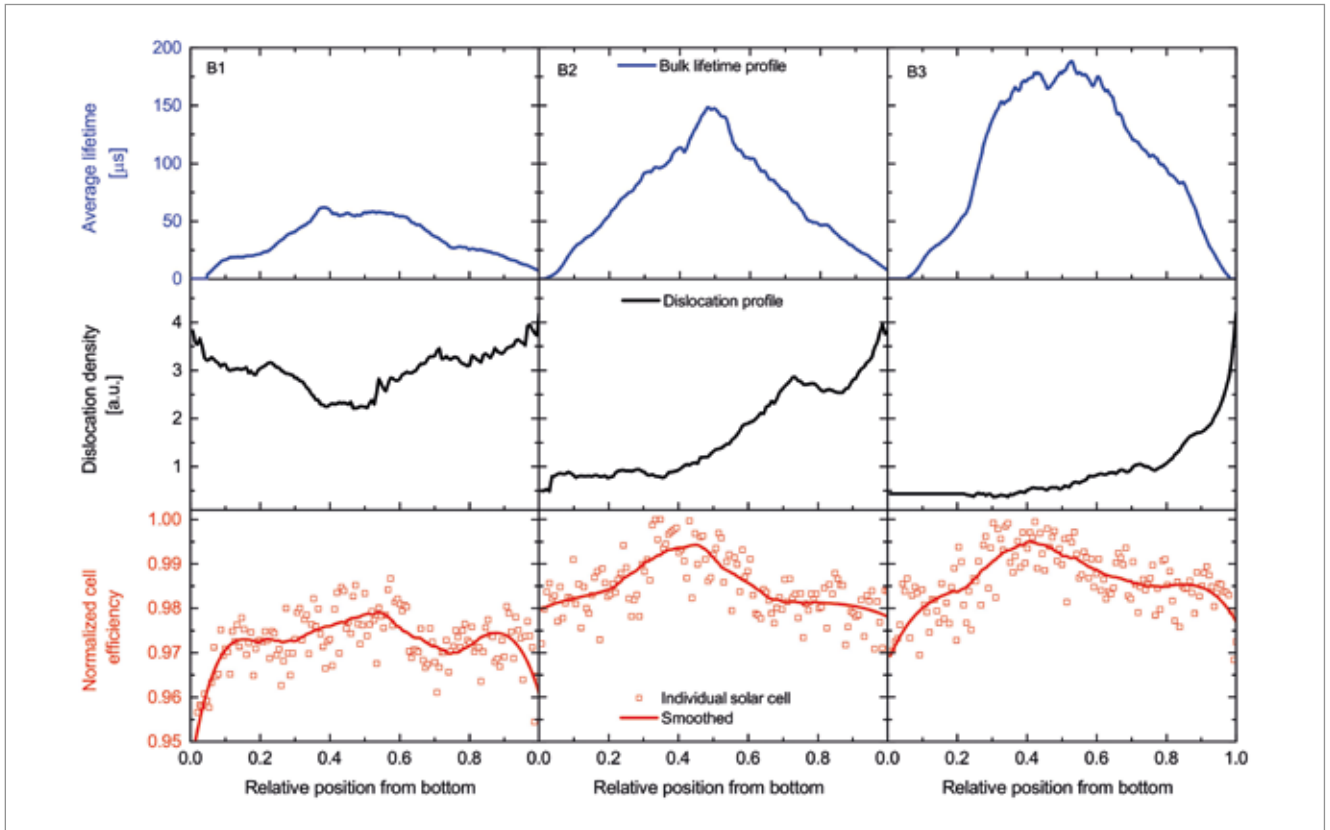


**Figure 3.** As-grown bulk lifetime from brick measurements, dislocation area fractions from wafer measurements, and PERC cell efficiencies along the height profile for bricks B1, B2 and B3. Lifetime data is represented by the harmonic mean from all pixels at a given height using Equation 1, at an injection level of  $1-8 \times 10^{18} \text{ cm}^{-3}$ , depending on the lifetime. The efficiency data is globally normalized to allow for comparisons between the three bricks, and a smoothed (polynomial fit?) curve is shown in the graphs. The spread of the data around the smoothed curve indicates the influence of the variability in cell processing and I-V measurements on the results.

‘random effect’ term for the bricks in order to allow the adjustment of the response ‘baseline’ for each brick. The combined model, for example, includes the bulk lifetime value and the wafer dislocation values, each with a single fitting parameter. A correlated random error term is included to account for the correlation between neighbouring wafers due to their physically sequential arrangement within the bricks. The model equation is:

$$y_{i,j} = \beta_0 + \beta_1 \tau_{i,j} + \beta_2 \delta_{i,j} + b_i + e_{i,j} \quad (1)$$

where

- $y_{i,j}$  = observed value of the response variable for observation  $j$  in brick  $i$  ( $i = 1, 2, 3$ );
- $\tau_{i,j}$  = harmonic mean of the observed bulk lifetime value;
- $\delta_{i,j}$  = dislocation value;
- $b_i$  = random effect for brick  $i$ , assumed to be normally distributed with zero mean and variance  $\sigma_b^2$ ;
- $e_{i,j}$  = random error, assumed to be normally distributed with zero mean and variance  $\sigma_e^2$ ;
- $\beta_0$  = overall intercept;
- $\beta_1, \beta_2$  = the fitted parameters.

Before using the linear mixed models, each data point was normalized by subtracting the global

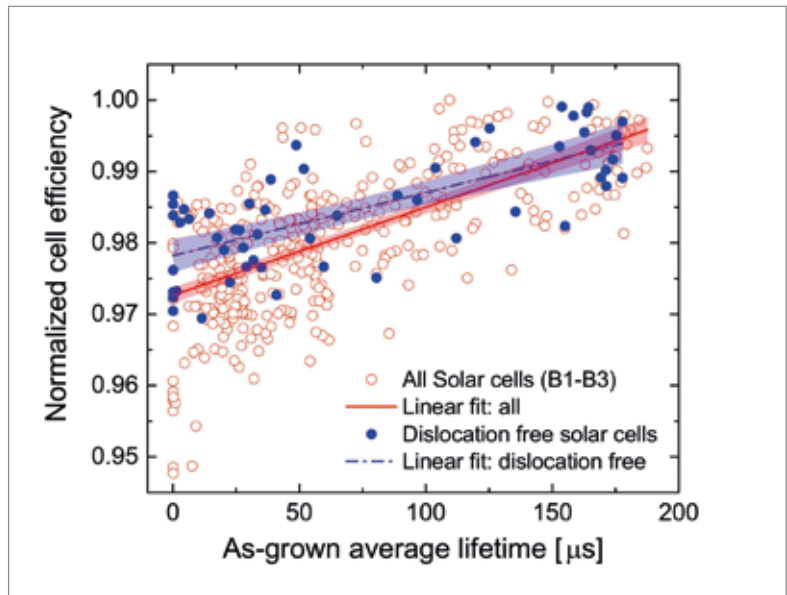


**Figure 4.** Correlation of cell efficiency, normalized to the highest-efficiency cell, and the harmonically averaged as-grown bulk lifetimes across the full sample set (red empty circles) and across the dislocation-free bottom half of brick B3 (blue filled circles). The shaded area is the standard error of the regression. Note that the bulk lifetime for the cell after processing is not known.

arithmetic mean and dividing by the global standard deviation for each of the data streams:  $\tau$ ,  $\delta$  and  $I_{sc} \times V_{oc}$ . The resulting units of the data points used in the fitting can be thought of as the number of standard deviations from the mean, where the mean

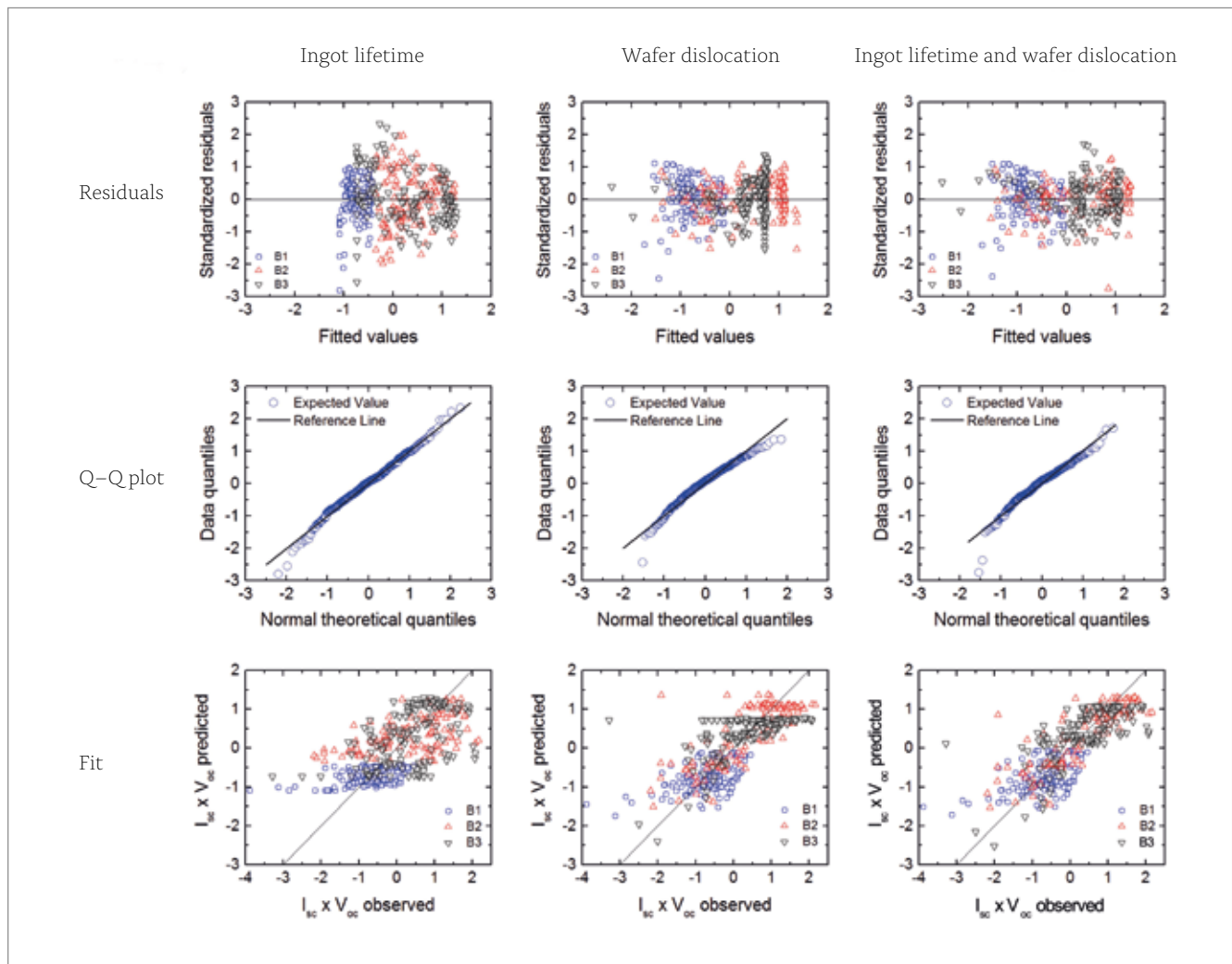


**Figure 5. Residuals, Q–Q plots and fitted vs. observed values for three models: lifetime only (left), wafer dislocation only (centre), and lifetime with wafer dislocation (right). All values are standardized, i.e. the axis values show unitless multiples of standard deviation above or below the respective mean values.**

“Respectable cell efficiencies are achieved even for very low-quality sections of the brick, as a result of substantial improvements in bulk lifetime during cell processing.”

is zero. This practice allows a fair comparison to be made between model equations and information, as presented graphically.

Three separate models are used here to investigate the influence of various measured variables on the measured response variable  $I_{sc} \times V_{oc}$  (see Equation 1); the specific variables are the lifetimes measured on the bricks, and the dislocation area fractions measured on the wafers.

First, the influence of lifetime alone is investigated, followed by the influence of the dislocation area fraction, as measured on the wafers. Finally, the models are compared using the two variables in additive combination. The model is a linear mixed-effects model, with a normal distribution assumption, fitted with the restricted maximum likelihood (REML) algorithm. Because of the spatially sequential

arrangement of wafers in each brick, an appropriate correlation structure has been fitted to the model errors  $e_{ij}$ . The correlation structure with the best fit (judged by likelihood ratio tests) is one which decays exponentially with the distance between the wafers. The same correlation structure is incorporated into all three models. Note that a standard linear model which neglects the correlation within the bricks and the random effect term resulted in similar best fits.

Graphs useful for assessing the assumptions in the models and for gauging the predictive ability of the fitted models are shown for each of the three models in Fig. 5. The plots of actual values vs. fitted curves allow the assumption of homoscedasticity (homogeneity of variance) to be assessed. This requirement appears to be satisfied for all three models. This is supported by Fig. 3, which shows that significant process-induced variance is observed, but appears uniformly spread across the data. The quantile–quantile (Q–Q) plots in Fig. 5 demonstrate the degree to which a normal distribution assumption holds; this appears to be satisfied by all three fitted datasets, which inspires confidence in drawing conclusions from these fitted datasets.

Variables	Ingot lifetime	Wafer dislocations	Ingot lifetime and wafer dislocations
Model number	1	2	3
AIC	813	773	752
P-value (fixed effects)	<0.001	<0.001	<0.001 (both)
Model 1 vs. Model 3			<0.001
Model 2 vs. Model 3			<0.001
RMSE	0.80	0.66	0.61

**Table 1. Akaike information criterion, p-values and root mean square error for the set of three models. Note that the RMSE value contains significant process-induced variance.**

From Table 1, the combined model (Model 3) is the preferred model, because it has the lowest Akaike information criterion (AIC) value compared with each of the single-predictor models. The AIC value measures the relative quality of each model for comparison purposes.

In Fig. 5 the data is gathered more tightly around the fitted line for Model 3 throughout the whole range. The results show that the correlation between lifetime and solar cell output parameter  $I_{sc} \times V_{oc}$  is statistically significant. However, for the model with lifetime only (Model 1) there is a ‘tail’ of sample values that are not well fitted by the model: these samples originate largely from the very bottom of the bricks.

It was found that the model that uses solely the variation of dislocation area fraction as measured on wafers provides a better fit than the model that relies on lifetime alone for this sample set. The model using dislocation as the only variable has smaller AIC and RMSE values than in the case of the model based on brick lifetime (see Table 1). However, in the bottom section of bricks B2 and B3, where the wafers are virtually dislocation free, the dislocation metric cannot be used to fit changes in  $I_{sc} \times V_{oc}$ . In this section of the brick, lifetime is the dominant metric. Unsurprisingly, the combined parameter model also proves to be a better model than both the models that rely on a single variable. This modelling demonstrates that lifetime has a significant influence on efficiency when used together with the dislocation information from the wafer measurements. With increasing improvements in wafer quality in terms of dislocation densities, and with increasing cell efficiencies, it is expected that, practically speaking, bulk lifetime will play an increasingly significant role in determining cell performance.

The modelling results indicate that lifetime and dislocation are partially correlated with each other, since Model 3 still has a lower AIC value than either Model 1 or Model 2.

### Conclusions and final remarks

As-grown bulk lifetimes derived from sPLIR measurements on mc-Si bricks have been found to have a statistically significant correlation with the performance, i.e. the  $I_{sc} \times V_{oc}$  product

“sPLIR can be used to select the best high-bulk-lifetime and low-dislocation silicon for high-efficiency lines.”

or the efficiency, in mc-Si PERC solar cells. For dislocation-free material, a good fit to a linear correlation between the as-grown bulk lifetime and the  $I_{sc} \times V_{oc}$  product is found.

Models based on fitting the dislocation metrics derived from PL images measured on as-cut wafers remain more statistically significant across the sample set studied here. However, with further reductions in the variability of dislocation area fractions of mc-Si, as-grown bulk lifetime will become more relevant; this is a global industry trend and is demonstrated in bricks 2 and 3 in this study. Quantitative brick inspection, in particular the bulk lifetime analysis based on sPLIR, will therefore play an important role for routine quality-control inspection in production, and for faster and more efficient process feedback in R&D.

In the short term, sPLIR can be used to select the best high-bulk-lifetime and low-dislocation silicon for high-efficiency lines. The unselected material can be sent to Al-BSF cell lines with very little negative impact on these lines, since this older cell process is less sensitive, especially to bulk lifetime. For manufacturers the cost of adding sPLIR for brick inspection would probably be more than offset by the gains in cell efficiencies in high-efficiency PERC lines. Additionally, the spatially resolved sPLIR results yield direct and detailed feedback for optimizing ingot growth parameters over solidification time. And as more-advanced mc-Si solidification processes become more widespread, the situation may arise where dislocations are so controlled that bulk lifetime, as measured on bricks, will be the only measurable material-related metric that impacts cell efficiency, and hence will be the primary metric for quality control and efficiency sorting. Importantly, the relevant lifetime range, with bulk lifetimes exceeding 100µs or even in the millisecond range, is not measurable using microwave-detected photoconductance decay (PCD)-based tools, which report effective lifetimes only.

**Acknowledgements**

This research has been supported by the Australian Government through the Australian Renewable Energy Agency (ARENA) Grants 7-Foo8 and RND009. The Australian Government does not accept responsibility for the views, information or advice expressed herein. The authors would like to thank R. Evans for fruitful discussions. This work has also been supported by the Natural Science Foundation of Jiangsu Province in China under Project No. BK20170057.

**References**

- [1] ITRPV 2017, "International technology roadmap for photovoltaic (ITRPV): 2016 results", 8th edn (Mar.) [<http://www.itrpv.net/Reports/Downloads/>].
- [2] Schmidt, J. & Bothe, K. 2004, "Structure and transformation of the metastable boron- and oxygen-related defect center in crystalline silicon", *Phys. Rev. B*, Vol. 69, No. 2, p. 24107.
- [3] Vargas, C. et al. 2017, "Recombination parameters of lifetime-limiting carrier-induced defects in multicrystalline silicon for solar cells", *Appl. Phys. Lett.*, Vol. 110, No. 9, p. 92106.
- [4] Herguth, A. et al. 2008, "Investigations on the long time behavior of the metastable boron-oxygen complex in crystalline silicon", *Prog. Photovolt: Res. Appl.*, Vol. 16, No. 2, pp. 135-140.
- [5] Hallam, B.J. et al. 2014, "Advanced bulk defect passivation for silicon solar cells", *IEEE J. Photovolt.*, Vol. 4, No. 1, pp. 88-95.
- [6] Dullweber, T. & Schmidt, J. 2016, "Industrial silicon solar cells applying the passivated emitter and rear cell (PERC) concept - A review", *IEEE J. Photovolt.*, Vol. 6, No. 5, pp. 1366-1381.
- [7] Min, B. et al. 2017, "A roadmap toward 24% efficient PERC solar cells in industrial mass production", *IEEE J. Photovolt.*, Vol. 7, No. 6, pp. 1-10.
- [8] Steinkemper, H., Hermle, M. & Glunz, S.W. 2016, "Comprehensive simulation study of industrially relevant silicon solar cell architectures for an optimal material parameter choice", *Prog. Photovolt: Res. Appl.*, Vol. 24, No. 10, pp. 1319-1331.
- [9] Demant, M. et al. 2016, "Inline quality rating of multi-crystalline wafers based on photoluminescence images", *Prog. Photovolt: Res. Appl.*, Vol. 24, No. 12, pp. 1533-1546.
- [10] Haunschild, J. et al. 2010, "Quality control of as-cut multicrystalline silicon wafers using photoluminescence imaging for solar cell production", *Sol. Energy Mater. Sol. Cells*, Vol. 94, No.

# PV Manufacturing & Technology Quarterly report



All the latest technology and manufacturing data from the industry's leading PV companies is provided by PV-Tech Research in a quarterly report. This includes forecasts for all leading manufacturers across different regions, cell types and shipment locations

PV-Tech's Market Research division provides the industry with accurate and timely data to allow PV manufacturers, and equipment and material suppliers, to understand existing and future technology landscapes and roadmaps.

More information:  
[marketresearch.solarmedia.co.uk](http://marketresearch.solarmedia.co.uk)

Contact us:  
[marketresearch@solarmedia.co.uk](mailto:marketresearch@solarmedia.co.uk)  
+44 (0) 207 871 0122

12, pp. 6–11.

[11] Deng, W. et al. 2016, “20.8% efficient PERC solar cell on 156 mm×156 mm p-type multi-crystalline silicon substrate”, *IEEE J. Photovolt.*, Vol. 6, No. 1, pp. 3–9.

[12] Wasmer, S. et al. 2017, “Impact of material and process variations on the distribution of multicrystalline silicon PERC cell efficiencies”, *IEEE J. Photovolt.*, Vol. 7, No. 1, pp. 118–128.

[13] Bothe, K. et al. 2010, “Determination of the bulk lifetime of bare multicrystalline silicon wafers”, *Prog. Photovolt: Res. Appl.*, Vol. 18, No. 3, pp. 204–208.

[14] Mitchell, B. et al. 2011, “Bulk minority carrier lifetimes and doping of silicon bricks from photoluminescence intensity ratios”, *J. Appl. Phys.*, Vol. 109, No. 8, pp. 83111–1–83111–12.

[15] Geerligs, L.J. 2003, “Impact of defect distribution and impurities on multicrystalline silicon cell efficiency”, *Proc. 3rd WCPEC*, Osaka, Japan.

[16] Gibaja, F. et al. 2013, “Silicon ingot quality and resulting solar cell performance”, *Energy Procedia*, Vol. 38, pp. 551–560.

[17] Mitchell, B., Chung, D. & Teal, A. 2016, “Photoluminescence imaging using silicon line-scanning cameras”, *IEEE J. Photovolt.*, Vol. 6, No. 4, pp. 967–975.

[18] Mitchell, B. et al. 2016, “Metrology at the ingot level : Addressing the growing importance of bulk material quality”, *Photovoltaics International*, 33rd edn, pp. 34–40.

[19] Mitchell, B. et al. 2017, “PERC solar cell performance predictions from multicrystalline silicon ingot metrology data”, *IEEE J. Photovolt.*, Vol. 7, No. 6, pp. 1619–1626.

[20] BT Imaging 2017, “LIS-B3: Production tool for silicon ingot and brick inspection” [<http://bit.ly/2gKFLZz>].

[21] R Core Team 2016, “R: A language and environment for statistical computing”, R Foundation for Statistical Computing, Vienna, Austria [<http://www.R-project.org/>].

[22] McLean, R., Sanders, W. & Stroup, W. 1991, “A unified approach to mixed linear models”, *Am. Stat.*, Vol. 43, No. 1, pp. 54–64.

[23] Oberg A.L. & Mahoney, D.W. 2007, “Linear mixed effects models”, *Methods Mol. Biol. Top. Biostat.*, Vol. 404, pp. 213–234.

[24] Pinheiro, J. et al. 2016, “nlme: Linear and nonlinear mixed effects models”, R package [<https://CRAN.R-project.org/package=nlme>].

[25] Mitchell, B. et al. 2014, “Imaging as-grown interstitial iron concentration on boron-doped silicon bricks via spectral photoluminescence”, *IEEE J. Photovolt.*, Vol. 4, No. 5, pp. 1185–1196.

[26] Schubert, M.C. et al. 2013, “Impact of impurities from crucible and coating on mc-silicon quality – The example of iron and cobalt”, *IEEE J. Photovolt.*, Vol. 3, No. 4, pp. 1250–1258.

[27] Wagner, H. et al. 2015, “Device architecture and lifetime requirements for high efficiency multicrystalline silicon solar cells”, *Energy Procedia*,

Vol. 77, pp. 225–230.

**About the Authors**

Bernhard Mitchell is a semiconductor physicist with more than 10 years’ experience in the PV sector, in both silicon and III-V technologies. He has worked at many leading PV research institutes around the world, including the University of Konstanz, UC Berkeley and Fraunhofer ISE, and has spent many years at UNSW Australia. He has developed a special expertise in metrology for silicon PV, and is now an R&D engineer with Wavelabs Solar Metrology Systems GmbH in Germany.

Daniel Chung is a Ph.D. student at the Australian Centre for Advanced Photovoltaics at UNSW Australia. His research focuses on the development of photoluminescence characterization of silicon ingots and applications in solar cell manufacturing.

Zhen Xiong is the chief engineer of ingot and wafer technology at Trina Solar. After graduating from the Chinese Academy of Sciences, he received his Ph.D. in 2010 and joined Trina Solar, where he focuses on research into silicon crystalline growth as well as the related characterization techniques.

Pietro P. Altermatt is the principal scientist at the State Key Laboratory for PV Science and Technology (SKL) at Trina Solar. In the 1990s he contributed to achieving the world-record PERL cell efficiencies at UNSW with numerical device modelling. He now equally successfully models mass-fabricated PERC cells, which are very similar in design to PERL cells.

Peter Geelan-Small is a biometrician with a background mainly in the area of natural resource management. He is currently a statistical consultant at UNSW, working in a broad range of areas, including projects from various engineering fields.

Thorsten Trupke is a semiconductor physicist with more than 15 years’ experience in R&D in the PV sector, and with an emphasis on the development of novel characterization methods. He is a professor at the Australian Centre for Advanced Photovoltaics at UNSW, and also a co-founder and the CTO of BT Imaging, a start-up company that commercializes PL imaging inspection systems.

**Enquiries**

Bernhard Mitchell  
Wavelabs Solar Metrology Systems GmbH  
Germany

Email: [b.mitchell@wavelabs.de](mailto:b.mitchell@wavelabs.de)